Optics Letters

Quantitative photoacoustic tomography by stochastic search: direct recovery of the optical absorption field

Mamatha Venugopal,[1] Peter van Es,[2] Srirang Manohar,[2] Debasish Roy,[3] and Ram Mohan Vasu[1,*]

[1]Optical Tomography Lab, Department of Instrumentation and Applied Physics, Indian Institute of Science, Bangalore-560012, Karnataka, India
[2]Biomedical Photonic Imaging, Mira Institute of Biomedical Technology and Technical Medicine, University of Twente, PB 217, 7500 AE Enschede, The Netherlands
[3]Computational Mechanics Lab, Department of Civil Engineering, Indian Institute of Science, Bangalore-560012, Karnataka, India
*Corresponding author: vasu@isu.iisc.ernet.in

Received 24 March 2016; revised 28 July 2016; accepted 9 August 2016; posted 10 August 2016 (Doc. ID 261637); published 8 September 2016

We present, perhaps for the first time, a stochastic search algorithm in quantitative photoacoustic tomography (QPAT) for a one-step recovery of the optical absorption map from time-resolved photoacoustic signals. Such a direct recovery is free of the numerical inaccuracies inherent in conventional two-step approaches that depend on an accurate estimation of the absorbed energy distribution. The absorption profile parameterized as a vector stochastic process is additively updated over time recursions so as to drive the measurement-prediction misfit to a zero-mean white noise. The derivative-free additive update is a welcome departure from the conventional gradient-based methods requiring evaluation of Jacobians at every recursion. The quantitative accuracy of the recovered absorption map from both numerical and experimental data is good with an overall error of less than 10%.

OCIS codes: (170.0170) Medical optics and biotechnology; (170.5120) Photoacoustic imaging; (170.3010) Image reconstruction techniques; (170.6960) Tomography.

http://dx.doi.org/10.1364/OL.41.004202

Photoacoustic tomography (PAT) is a noninvasive hybrid technique combining high optical contrast with superior ultrasound resolution in imaging soft tissues [1,2]. The absorption of short near-infrared (NIR) pulses (700–1100 nm) primarily by cancerous regions generates sources of pressure in the object through heating and thermo-elastic expansion. The initial pressure rise propagates across the tissue as an acoustic wave and is recorded by wideband ultrasonic transducers resident outside the tissue [3]. In order to simulate the received photoacoustic (PA) signal, apart from the basic PA process, one needs two propagation models: one for light and the other for the acoustic waves. The ultimate goal of PAT is to invert the time-resolved PA signals to recover the optical absorption coefficient map that can directly provide functional images [4]. This is usually done in a two-step process: the first step reconstructs the acoustic sources or equivalently the absorbed energy map, $h(\mathbf{r})$, which is proportional to the product of the optical absorption coefficient, $\mu_a(\mathbf{r})$, and the integrated optical fluence, $\phi(\mathbf{r})$, within the pulse; the second step reconstructs $\mu_a(\mathbf{r})$ from $h(\mathbf{r})$. A major limitation of a two-step process stems from the dependence of $h(\mathbf{r})$ on the optical source positions. Consequently, increasing the number of source-detector views to tackle the so-called ill-posedness unwittingly increases the dimension of the problem and aggravates the situation further. A direct recovery of μ_a is ideal as the invariance of this parameter, with respect to the source locations, keeps the number of unknowns unchanged. Notwithstanding this and other advantages [5] and the significance of $\mu_a(\mathbf{r})$ in functional and diagnostic imaging, research effort in PAT has mostly been on developing algorithms for the recovery of $h(\mathbf{r})$ [6–8]. A direct recovery of $\mu_a(\mathbf{r})$ from the PA measurements renders the inverse problem nonlinear and has not yet been attempted in time-domain PAT. A possible reason could be the computationally intensive Jacobian calculations demanded in gradient-based techniques, commonly employed *en route* to solving such nonlinear inverse problems. The limited work on quantitative PAT (QPAT), reported in the literature, either lacks an algorithm for direct μ_a recovery or has not been tested satisfactorily under clinically relevant conditions [9–15]. Although a direct recovery of μ_a has been attempted in the frequency-domain [5,16,17], it has since been pointed out that the reconstructions obtained in the time-domain have better quantitative accuracy and signal-to-noise ratio [18]. The present work puts forth an evolutionary stochastic search algorithm, fashioned after the principles of generalized Bayesian updates, that enables a direct recovery of the optical absorption map from the recorded PA signals. Within a Bayesian setting, the parameters to be recovered are treated as random variables and the *a priori* information, if any, available on the parameters could be incorporated in their prior distributions [19]. Ideally, each realization (also called a particle) from the prior distribution is assigned a corresponding weight which reflects the error

between the available measurements and the predictions from the forward model. The particle-weight pair constitute the update, wherein the best fit realization attains the highest weight and vice versa. In such a scheme, the whole weight could be asymptotically assigned to a single particle thereby disabling any non-trivial updates. Prevention of such "particle impoverishment" or weight degeneracy, and hence of the contingency of a prematurely converged incorrect solution, generally necessitates an exponential increase of ensemble size with increasing system dimension [20]. Such a scenario is avoided in our search algorithm by converting the multiplicative weights into additive corrections to be applied to the particle locations in the parameter space [21].

The time evolution of PA wave fields can be modeled using equations of linear acoustics. For soft biological tissues, it is assumed that the medium is isotropic and quiescent, the pressure flow is irrotational and the shear waves are negligible [7]. The wave propagation equation in a lossless medium, $\mathbf{D}$, may then be written as

$$\nabla^2 p(\mathbf{r}, t) - \frac{1}{c^2}\frac{\partial^2 p(\mathbf{r}, t)}{\partial t^2} = 0, \tag{1}$$

with the initial condition $\partial p_0(\mathbf{r})/\partial t = 0$, where $p_0(\mathbf{r})$ is the initial pressure rise, c is the speed of sound in the medium, and $p(\mathbf{r}, t = 0) := p_0(\mathbf{r})$. Moreover, $p_0(\mathbf{r})$ is related to $\mu_a(\mathbf{r})$ through

$$p_0(\mathbf{r}) = \left(\frac{\beta c^2}{C_p}\right)\mu_a(\mathbf{r})\phi(\mathbf{r}) = \Gamma h(\mathbf{r}), \tag{2}$$

where β is the isobaric volume expansion coefficient, C_p is the specific heat and $\Gamma = \beta c^2/C_p$ is the Grüneisen coefficient. The wave equation is solved along with an absorbing boundary condition (BC), [18] which is $\nabla p(\mathbf{r}, t)\cdot\mathbf{n} = -\frac{1}{c}\frac{\partial p(\mathbf{r},t)}{\partial t} - \frac{p(\mathbf{r},t)}{2r}$, where $\mathbf{n}$ is the unit normal to the boundary, $\partial\mathbf{D}$, and r, the object radius. The integrated optical fluence $\phi(\mathbf{r})$ in Eq. (2) is the solution to the photon diffusion equation (DE) [22]:

$$-\nabla.\kappa\nabla\phi(\mathbf{r}) + \mu_a(\mathbf{r})\phi(\mathbf{r}) = S(\mathbf{r}), \tag{3}$$

and Robin BC, $\phi(\mathbf{r}) + 2\kappa A\frac{\partial\phi(\mathbf{r})}{\partial\mathbf{n}} = 0$ [22]. (Since the timescale at which an acoustic response is generated is approximately three orders of magnitude larger than the timescale of the optical pulse, we note that only the time-independent $\phi(\mathbf{r})$ needs to be propagated, which obeys the continuous wave DE.) Here, A is the Fresnel reflection coefficient, κ is the diffusion coefficient given by $\kappa = [3(\mu_a + \mu_s')]^{-1}$ where μ_s' is the reduced scattering coefficient, and $S(\mathbf{r})$ is the strength of the incident optical source. The forward model described by Eqs. (1)–(3), coupled with the corresponding BCs is discretized using the finite element method to arrive at $\{\mathbf{p}_{t_i}\}_{i=1}^{n_t} = \mathcal{F}(\boldsymbol{\mu})$, where $\mathbf{p} := p(\mathbf{r}), \boldsymbol{\mu} := \mu_a(\mathbf{r})$, $\mathbf{r}\in\mathbf{D}$ and $t_1, \ldots, t_{n_t}$ are the sampling time points at which measurements are recorded. The details of the basis functions used in the finite element discretizations of the acoustic and optical models may be found in Refs. [18,22].

The inverse problem of QPAT is to recover $\boldsymbol{\mu}$ from a finite set of boundary measurements, $p(\mathbf{r}', t)$, $\mathbf{r}'\in D'\subset\partial\mathbf{D}$, henceforth denoted as $\{\mathbf{m}_{t_i}\}_{i=1}^{n_t}$. Let $\boldsymbol{\mu}\in\mathbb{R}^{n_\mu}$ and $\mathbf{m}_{t_i}\in\mathbb{R}^{n_m}$ $\forall\ i = 1, \ldots, n_t$, where n_μ is the number of nodes in the finite element discretization of the object, $\mathbf{D}$, and n_m, the number of detectors placed around it. Our stochastic search approach to solve the inverse problem, similar to any other Bayesian scheme [20], consists of a prediction-update strategy applied to a set of realizations of the parameter random vector at every iteration [19,21]. However, in order to assimilate the time-varying PAT data, here, the parameter vector is modeled as a stochastic process rather than a vector random variable having no temporal evolution. Nevertheless, being inherently non-dynamic in nature, the parameter vector must also be so evolved as to attain, perhaps asymptotically, a time-invariant steady state upon assimilating all the available data. Thus as a first step in constructing the Bayesian update dynamics, temporal fluctuations in the parameter vector are modeled using a Brownian motion:

$$\boldsymbol{\mu}_{t_{i+1}} = \hat{\boldsymbol{\mu}}_{t_i} + \Delta\mathbf{B}_{t_i}, \tag{4}$$

where $\boldsymbol{\mu}_{t_{i+1}}$ and $\hat{\boldsymbol{\mu}}_{t_i}$ denote the predicted and updated parameter vectors respectively at times t_{i+1} and t_i, $\Delta\mathbf{B}_{t_i} = \mathbf{B}_{t_{i+1}} - \mathbf{B}_{t_i}$, and $\mathbf{B}_t\in\mathbb{R}^{n_\mu}$ is a Brownian motion with mean zero and covariance $\sigma_B\sigma_B^T\in\mathbb{R}^{n_\mu\times n_\mu}$. The measurement equation mapping the optical absorption to the boundary pressure may be written as

$$\mathbf{m}_{t_{i+1}} = \mathcal{F}(\boldsymbol{\mu}_{t_{i+1}}) + \mathbf{W}_{t_{i+1}}, \tag{5}$$

where $\mathcal{F}$ describes the operator which converts the input absorption profile into a pressure distribution on the boundary using Eqs. (1)–(3) and $\mathbf{W}_t\in\mathbb{R}^{n_m}$ is the measurement noise with mean zero and covariance $\sigma_W\sigma_W^T\in\mathbb{R}^{n_m\times n_m}$.

The stochastic search (SS) for a nonlinear problem is implemented in a Monte Carlo (MC) setup at the time instants when the measurements are available, that is, at $t_1, \ldots, t_{n_t}$. Let the initial ensemble of $\boldsymbol{\mu}$, that is, $\{\hat{\boldsymbol{\mu}}_0(j)\}_{j=1}^{n_e}$ be generated from a prior distribution, say a uniform or Gaussian distribution. Here, n_e denotes the ensemble size. Then, given the updated ensemble, $\{\hat{\boldsymbol{\mu}}_i(j)\}_{j=1}^{n_e}$, at time, t_i, the SS should be in the form of a recursive prediction-update scheme to arrive at $\{\hat{\boldsymbol{\mu}}_{i+1}(j)\}_{j=1}^{n_e}$. Note that, for notational convenience, the subscript t_i has been replaced by i and so on. The particle-wise prediction equation follows from Eq. (4) as

$$\boldsymbol{\mu}_{i+1}(j) = \hat{\boldsymbol{\mu}}_i(j) + \Delta\mathbf{B}_i(j), \qquad j = 1, \ldots, n_e. \tag{6}$$

The update step assimilates the available measurements to estimate the posterior parameter distribution and in the process, drives the measurement-prediction misfit (or the innovation vector), $\mathbf{m}_t - \mathcal{F}(\boldsymbol{\mu}_t)$, to a zero-mean noise. Kalman filters [23] provide optimal state estimates when the measurements are linear and Gaussian. The current update has a structure similar to the Kalman update and may be considered a nonlinear ensemble version of the same [21,24,25]. Specifically, the update equation is given by

$$\hat{\boldsymbol{\mu}}_{i+1}(j) = \boldsymbol{\mu}_{i+1}(j) + \mathbf{G}_{i+1}(\mathbf{m}_{i+1} - \mathcal{F}(\boldsymbol{\mu}_{i+1}(j))),$$
$$j = 1, \ldots, n_e, \tag{7}$$

where $\mathbf{G}\in\mathbb{R}^{n_\mu\times n_m}$ is a gain matrix given by $\mathbf{G}_{i+1} = \mathbf{Q}_{i+1}\mathbf{R}_{i+1}^T(\mathbf{R}_{i+1}\mathbf{R}_{i+1}^T + \sigma_W\sigma_W^T)$. Here $\mathbf{Q}\in\mathbb{R}^{n_\mu\times n_e}$ and $\mathbf{R}\in\mathbb{R}^{n_m\times n_e}$ are the parameter and measurement ensemble perturbation matrices, respectively. Specifically, $\mathbf{Q}_{i+1} = \frac{1}{\sqrt{n_e-1}}[\boldsymbol{\mu}_{i+1}(1) - \frac{1}{n_e}\sum_{j=1}^{n_e}\boldsymbol{\mu}_{i+1}(j), \ldots, \boldsymbol{\mu}_{i+1}(n_e) - \frac{1}{n_e}\sum_{j=1}^{n_e}\boldsymbol{\mu}_{i+1}(j)]$. The expression for $\mathbf{R}_{i+1}$ may be obtained by replacing $\boldsymbol{\mu}_{i+1}$ with $\mathcal{F}(\boldsymbol{\mu}_{i+1})$ in $\mathbf{Q}_{i+1}$. The form of the right hand side of Eq. (7) is reminiscent of a quasi-Newton update with $\mathbf{G}_{i+1}$ apparently playing the role of a regularized Frèchet derivative, even though its evaluation here requires only sample moment information and no derivatives. The parameter estimate at

any time instant may be computed as the empirical mean given by

$$\bar{\boldsymbol{\mu}}_{i+1} = \frac{1}{n_e}\sum_{j=1}^{n_e}\hat{\boldsymbol{\mu}}_{i+1}(j). \tag{8}$$

A more detailed exposition of the proposed scheme may be found in Ref. [21]. Nevertheless, a step-by-step algorithm is given below for further clarity.

Algorithm

Given the set of measurements, $\mathbf{m}_i = (m_i^1, \ldots, m_i^{n_m})$ at any time instant t_i, the objective is to estimate the parameter vector, $\bar{\boldsymbol{\mu}}_i = (\bar{\mu}_i^1, \ldots, \bar{\mu}_i^{n_\mu})$. Input the covariance matrices, $\sigma_B\sigma_B^T$ and $\sigma_W\sigma_W^T$. Presently, they are scalar matrices with small positive entries. Also, set the ensemble size, n_e.

1. Generate the initial ensemble of parameters, $\{\hat{\boldsymbol{\mu}}_0(j)\}_{j=1}^{n_e}$, say from a Gaussian prior with zero mean and an assumed covariance. Set $i = 0, t_0 = 0$.
2. Propagate the parameter process to time t_{i+1} using Eq. (6).
3. Input each realization of the parameter process, $\boldsymbol{\mu}_{i+1}(j), j = 1, \ldots, n_e$ to the forward model described by Eqs. (1)–(3) and solve using the finite element method to compute $\mathcal{F}(\boldsymbol{\mu}_{i+1}(j)), j = 1, \ldots, n_e$.
4. Compute the ensemble perturbation matrices $\mathbf{Q}_{i+1}$ and $\mathbf{R}_{i+1}$ and then use them to compute the gain matrix, $\mathbf{G}_{i+1}$.
5. Update each realization, $\{\boldsymbol{\mu}_{i+1}(j)\}_{j=1}^{n_e}$, using Eq. (7).
6. Obtain the parameter estimate, $\bar{\boldsymbol{\mu}}_{i+1}$, using Eq. (8).
7. Set $i \to i+1$. If $i = n_t$, terminate the algorithm; otherwise, go to step 3.

For the numerical simulations, we first consider a circular object of radius 12 mm with three anomalous inclusions of radii 1 mm each as shown in Fig. 1(a). The background μ_a is 0.01 mm^{-1} and μ_s' is 1 mm^{-1} throughout the object, making it a predominantly scattering medium. The lower two inclusions have a μ_a of 0.05 mm^{-1}, while that of the upper one is 0.04 mm^{-1}. Γ is assumed to be 1 and c is 1500 ms^{-1}. The object is illuminated laterally generating a non-uniform fluence distribution inside as evident from the absorbed energy map in Fig. 1(b). This indicates that an $h(\mathbf{r})$ recovery would have provided an inaccurate quantitative distribution of the absorbers, and this is also clear from the relative contrast of the central anomaly in Fig. 1(b). To record the PA signals, 384 detectors are placed equidistant at a radius of 50 mm from the center of the object. Here, the medium between the object and the detectors is assumed to be water, as in our experiments. The signals were collected for a total duration of 60 μs at a sampling rate of 50 MHz. The 'numerical measurements' were generated by adding 1% Gaussian noise to the recorded PA waves and convolving the resulting noisy signals with a Gaussian filter centered at 5 MHz to simulate the response of our actual detectors. While we used a mesh consisting of 7633 nodes and 14976 triangular elements to generate the measurements, the reconstructions are performed on a coarser mesh of 1243 nodes and 2376 elements. Figure 2(a) shows the reconstructed μ_a map with a cross-sectional plot given in Fig. 2(b). We also employ the proposed scheme to compare our results with a two-step recovery, the details of which may be found in Ref. [14]. For brevity, we only show the cross-sectional plots of the two-step recovery in Fig. 2(b). Clearly, a direct recovery results in a better quantitative accuracy, especially at the center, since it avoids the pitfalls of a non-uniform fluence distribution apparent in a two-step scheme [see also Fig. 1(b)]. A two-step method also causes μ_a to overshoot near the boundary owing to the numerical division of $h(\mathbf{r})$ by $\phi(\mathbf{r})$.

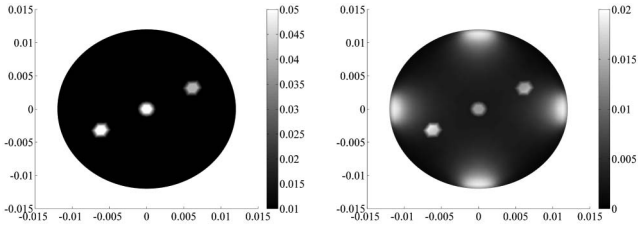

(a) (b)

Fig. 1. (a) μ_a map of the numerical object taken as the reference. For all grayscale μ_a images, the x and y axes are in m, and the color map is in mm^{-1}. (b) The absorbed energy map in Jm^{-3} of the numerical object.

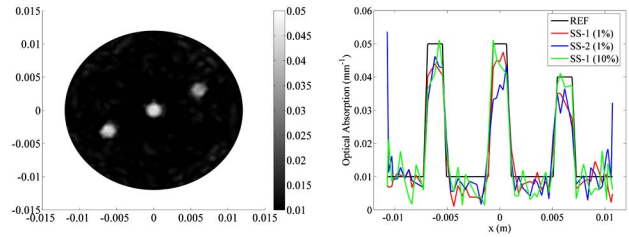

(a) (b)

Fig. 2. (a) Reconstructed μ_a map corresponding to the object in Fig. 1(a) for the 1% noise case and (b) the cross-sectional plot through $x = 2y$ comparing the results of a direct recovery (SS-1) and a two-step method (SS-2) for the 1% noise case. Also shown in the same figure is the cross-sectional plot corresponding to a one-step recovery for the 10% noise case.

In order to study the effect of measurement noise on the recovered image, we also invert measurements generated as above, but with 4%, 7%, and 10% Gaussian noises. For brevity again, only a cross-section of the reconstruction for the 10% noise case is given in Fig. 2(b). Our next numerical object is the more complex Shepp–Logan phantom (SLP), as shown in Fig. 3(a). The numerical setup for the SLP data generation is the same as in the previous case. While the forward data is generated on a mesh consisting of 14,893 nodes and 29,376 elements, the reconstruction is performed on a coarser mesh of 4903 nodes and 9576 elements. A one-step reconstruction of the SLP for the 1% noise case is given in Fig. 3(b).

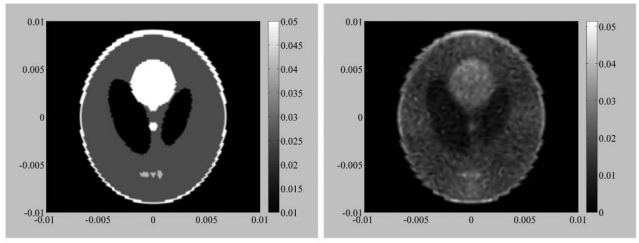

(a) (b)

Fig. 3. (a) μ_a map of the Shepp–Logan phantom (SLP). (b) Reconstructed μ_a map of the SLP using the one-step method.

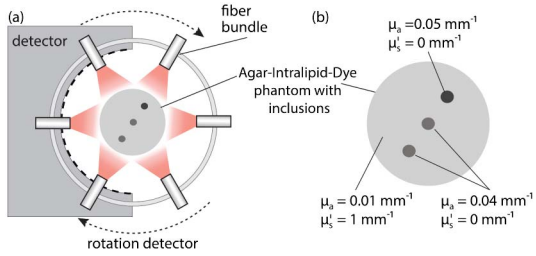

Fig. 4. (a) Schematic representation of the experimental setup. The phantom is illuminated with six static optical fiber bundles carrying 6 ns pulses at 800 nm. The 64-element curved ultrasound detector (5 MHz, 4 cm radius) rotates around the phantom and measures the PA signals in six views. (b) Schematic diagram and optical properties of the experimental phantom. The background material is agar gel with an aqueous solution of Intralipid and dye. The cylindrical inclusions were made from agar and an aqueous solution of dye without Intralipid.

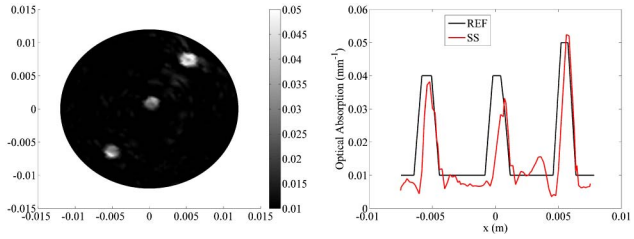

Fig. 5. (a) Reconstructed μ_a map and (b) the cross-sectional plot through $y = 1.26x$ corresponding to the experimental phantom.

A schematic representation of the experimental setup and the object, with its optical properties is in Fig. 4. We have considered a small-size phantom, keeping in mind small animal imaging and also our ongoing work on human finger-joint imaging [26]. Also, the choice of the 800 nm wavelength is to ensure high penetration depth as might be required in animal oncology research. At each detector, the signals are recorded for a duration of 44.56 μs at a sampling rate of 50 MHz. The reconstructions were performed on a mesh consisting of 2773 nodes and 5376 elements using an ensemble size of 800, the same as that used for the numerical simulations. Although it took 3.5 h on a hexacore i7 machine for the inversion to finish, a properly configured multi-processor cluster system will require only a few minutes or perhaps less. The reconstructed μ_a map of the phantom and a cross-sectional plot are shown in Figs. 5(a) and 5(b), respectively. The estimated absorption values of the anomalies were 0.038 mm^{-1}, 0.034 mm^{-1}, and 0.052 mm^{-1} resulting in errors of 5%, 17.5%, and 5%, respectively. Note that the results reported here are insensitive to the initial distribution of $\boldsymbol{\mu}$, unlike those reported in Ref. [5], where the reconstructions, based on a regularized Gauss–Newton search, though similar in quantitative accuracy, showed sensitive dependence on the initial absorption profile.

In conclusion, we have reported a SS algorithm for the direct recovery of the optical absorption map from the measured acoustic pressure. A key aspect of this work is the proposal of an easy-to-implement, derivative-free numerical scheme, the first of its kind for one-step QPAT. A possibly naive, if straightforward, extension of this work could be to recover the chromophore concentrations in tissues by gathering the PA data at multiple optical wavelengths and solving for μ_a at each wavelength. But then, such a two-step process would have similar ill-posedness issues as discussed earlier since the optical absorption varies with wavelength. In the future, we intend to address this issue through a one-step recovery of the chromophore concentrations from spectral PA data. Additional constraints appearing in the recovery of functional parameters such as the total hemoglobin concentration may be readily incorporated within the innovation vector of the proposed update scheme. This should again be contrasted with gradient-based approaches requiring regularization to incorporate such constraints, thus adding to the computational overhead caused by the Jacobian calculations.

Funding. Department of Science and Technology, Ministry of Science and Technology (DST), India; Netherlands Organization for Health Research and Development (ZonMw).

Acknowledgment. We thank Dr. Altaf Hussain for his assistance and for the use of his experimental setup.

REFERENCES

1. A. A. Oraevsky and A. A. Karabutov, *Biomedical Photonics Handbook*, T. Vo-Dinh, ed. (CRC Press, 2003).
2. L. V. Wang and S. Hu, Science **335**, 1458 (2012).
3. H. F. Zhang, K. Maslov, G. Stoica, and L. V. Wang, Nat. Biotechnol. **24**, 848 (2006).
4. P. Beard, Interface Focus **1**, 602 (2011).
5. Z. Yuan and H. Jiang, Med. Phys. **39**, 6895 (2012).
6. M. Xu and L. V. Wang, Phys. Rev. E **71**, 016706 (2005).
7. B. E. Treeby and B. T. Cox, J. Biomed. Opt. **15**, 021314 (2010).
8. X. L. Dean-Ben, V. Ntziachristos, and D. Razansky, IEEE Trans. Med. Imaging **31**, 1154 (2012).
9. M. Haltmeier, L. Neumann, and S. Rabanser, Inverse Probl. **31**, 065005 (2015).
10. N. Song, C. Deumié, and A. Da Silva, Biomed. Opt. Express **5**, 3960 (2014).
11. T. Tarvainen, A. Pulkkinen, B. T. Cox, J. P. Kaipio, and S. R. Arridge, IEEE Trans. Med. Imaging **32**, 2287 (2013).
12. G. Bal and K. Ren, Inverse Probl. **27**, 075003 (2011).
13. A. Q. Bauer, R. E. Nothdurft, T. N. Erpelding, L. V. Wang, and J. P. Culver, J. Biomed. Opt. **16**, 096016 (2011).
14. B. Banerjee, S. Bagchi, R. M. Vasu, and D. Roy, J. Opt. Soc. Am. A **25**, 2347 (2008).
15. A. Rosenthal, D. Razansky, and V. Ntziachristos, IEEE Trans. Med. Imaging **28**, 1997 (2009).
16. L. Yao, Y. Sun, and H. Jiang, Opt. Lett. **34**, 1765 (2009).
17. Z. Yuan and H. Jiang, Appl. Phys. Lett. **88**, 231101 (2006).
18. L. Yao and H. Jiang, J. Opt. A **11**, 085301 (2009).
19. F. C. Klebaner, *Introduction to Stochastic Calculus with Applications* (Imperial College, 2005).
20. M. S. Arulampalam, S. Maskell, N. Gordon, and T. Clapp, IEEE Trans. Signal Process. **50**, 174 (2002).
21. J. Teresa, M. Venugopal, D. Roy, R. M. Vasu, and R. Kanhirodan, J. Opt. Soc. Am. A **31**, 996 (2014).
22. S. R. Arridge, Inverse Probl. **15**, R41 (1999).
23. R. E. Kalman, Trans. ASME Ser. D J. Basic Eng. **82**, 35 (1960).
24. D. M. Livings, S. L. Dance, and N. K. Nichols, Phys. D **237**, 1021 (2008).
25. G. Evensen, Ocean Dynam. **53**, 343, 2003.
26. P. van Es, S. K. Biswas, H. J. Bernelot Moens, W. Steenbergen, and S. Manohar, J. Biomed. Opt. **19**, 060501 (2014).